Proceedings of DETC'04
2004 ASME Design Engineering Technical Conferences
Salt Lake City, Utah, USA, September-October 28-2, 2004

DETC2004-57406

DRAFT

A PARALLEL 5 DOF POSITIONER FOR SEMI-SPHERICAL WORKSPACES

Benjamin Maurin, Bernard Bayle
Jacques Gangloff, Michel de Mathelin
LSIIT (UMR CNRS-ULP 7005), Strasbourg I University
Bd. S. Brant, BP 10413, 67412 Illkirch cedex, FRANCE
Email: maurin@eavr.u-strasbg.fr

Olivier Piccin
LICIA(EA3434), INSA-Strasbourg
24, Bd de la Victoire, 67084 Strasbourg, FRANCE
Email: Olivier.Piccin@insa-strasbourg.fr

ABSTRACT

In this paper, we describe and model a new five-degree-of-freedom parallel manipulator. This structure has been specially designed for medical applications that require in the same time mobility, compactness and accuracy around a functional point. The purpose of this robotic device is to help practitioners in performing accurate needle insertion while preserving them from harmful intra-operative X-rays imaging devices. The system is built from revolute joints, among which only five joints are actuated to convey the required five degrees of freedom to its moving platform. A numerical simulation of the workspace and a real prototype are presented.

INTRODUCTION

Because surgery is changing very fast, new medical devices are always needed to solve difficult tasks. In medical cares, percutaneous procedures are among the upcoming treatments that can help the patient to have faster recovery and less painful interventions. Such interventions are commonly used for therapy or diagnosis by radiologists [1]. They consist in inserting a needle in the body of a patient through an entry point on the skin. Because of positioning accuracy requirements, these interventions are often done with intra-operative X-rays imaging devices such as Computed Tomography scans (CT-scan). Thus the practitioner may be exposed to large amounts of X-rays which are harmful for his health. Robotic assistants are a very promising solution for this kind of interventions since they could allow the protection of the practitioner while guarantying satisfactory accuracy. Such robotic systems working in the CT-scan ring already exist [2–4] and clinical trials have already been achieved. But these systems are not well suitable for every kind of percutaneous procedures, in particular for abdominal interventions for which the breathing of the patient has a great influence. In order to design a new robotic system, we list the very strong medical requirements for this kind of procedures. We present some of the most important constraints here (the reader will find further details in the literature [5, 6]). Additionally, the nature of the working environment (X-rays) will give different kind of constraints on the mechanism of the robotic system.

Required Mobility of the Mechanism. To mimic the radiologist gesture, we theoretically need six degrees of freedom to hold and insert the needle. But, from a practical point of view, we dissociate the positioning and orientation of the needle from the insertion itself. Indeed, it allows more safety during the insertion as the positioning and orientation will be accomplished by the robotic device described in this paper. The required mobility thus corresponds to three degrees for positioning the entry point and two additional degrees for orienting the line supporting the needle axis (no self rotation). The insertion task will be achieved by a tool mounted as an end-effector on the robotic device. The description of this specific tool is out-of-scope of this document.

Dimensions of the CT-scan Gantry. A CT-scan imaging device looks like a bulky horizontal-axis ring of 700 mm in diameter. The patient is placed on a translating table that moves through the ring, leaving only a small space available for special instruments. This is mainly due to the fact that CT-scans are not designed for medical interventions. The typical free space for the radiologist is thus a 200 mm radius half-sphere centered on the entry point.

CT Image Plane. Computed tomography works by acquiring numerous X-rays projections of its inner space, which is often called a CT-plane. This plane has a few millimeters width (10 to 30 mm) and vertically slices the patient body. As X-rays are very disrupted by metal and electrical devices, these materials must be avoided in the CT-plane. Since the mechanism has to hold the needle while the imaging device is acquiring a slice of the patient body, we must design our robot so that no metal parts cross the CT-plane.

Patient Safety, Exerted Forces and Accuracy. Safety and sterilization are critical requirements. Briefly, we can say that our system has to be attached to the patient body to avoid the breathing issue. It means that the robot is placed inside the CT ring and that it must be small enough to fit in the 200 mm half sphere. Furthermore, the robot must remain motionless in case of a failure in order to avoid an undesirable motion or twist of the needle. In [7] and our own experiments [8], we found that a maximum force of 20 N has to be applied on the needle during an insertion. This is a challenging constraint: in the same time the practitioner wants to have a precision of at least 1 mm. So, the accuracy and the rigidity of the system are other critical requirements.

Choice of the Structure. The design constraints we presented above limit the choice among the existing known mechanisms. We chose a parallel structure since these mechanisms are very well suited for absolute positioning accuracy and rigidity. Their workspaces are rather small when high mobility is required. As the combination of serial mechanism and parallel structure may help to find a good compromise, this is the choice we finally made.

The paper is organized as follows. In the first section the robot is described using a local product of exponential representation and the closed-chain model is given. In the second section we calculate the forward and inverse kinematic models. Finally, in the last section we give simulation results (notably the workspace representation) and present the prototype built from our study.

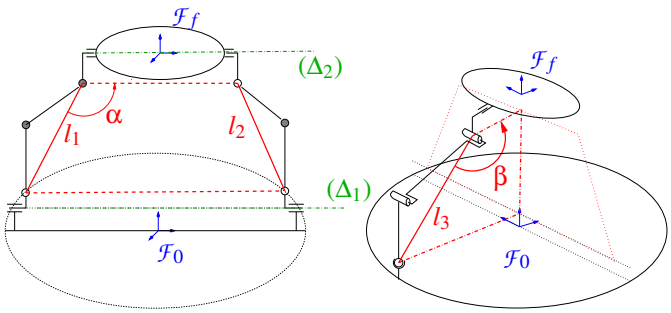

(a) THE 6-BAR LINKAGE (l_1,l_2,α), legs 1 and 2.

(b) THE 4-BAR LINKAGE (l_3,β), leg 3.

Figure 1. SIMPLIFIED REPRESENTATION

DESCRIPTION OF THE MECHANISM

Our design is inspired by the work of Hunt [9] on the geometry of mechanisms. Tsai [10] proposes a methodology for creating and classifying mechanisms. According to this classification, the system we designed is made of one 6-bar linkage associated to a 4-bar linkage joined together by a common platform.

Structure Description

The structure has three legs, *i.e.* three serial chains joining the base to the platform. A frame $\mathcal{F}_0 = (O_0, \mathbf{x_0}, \mathbf{y_0}, \mathbf{z_0})$ is associated to the base of the robot and a frame $\mathcal{F}_f = (O_f, \mathbf{x_f}, \mathbf{y_f}, \mathbf{z_f})$ is associated to the platform (see Fig. 1). The first two opposite legs of the robot are symmetrical chains and form the planar 6-bar linkage. This linkage aims at constraining three degrees of freedom in its plane (Fig.1(a)). The three controlled parameters associated to this 6-bar linkage are the variable lengths l_1, l_2 and the angle α.

Once these two legs are positioned, two degrees of freedom have to be defined: the first one is a rotation of the planar 6-bar linkage about the line (Δ_1) passing through the base (Fig. 1(a)). The second corresponds to a platform rotation about the line (Δ_2).

Geometrically, the mechanism constraints any fixed point of the platform to move on a circle contained in a plane normal to the line (Δ_1). In addition, the platform orientation is possible through a rotation about the same line (Δ_1). Finally, the last leg must constraint these two degrees of freedom with the variable length l_3 and angle β (Fig. 1(b)).

Our real model includes a more complex structure for each leg to have all the benefits of a parallel structure together with the workspace of a serial robot. We used only revolute joints in the design (see Fig. 2).

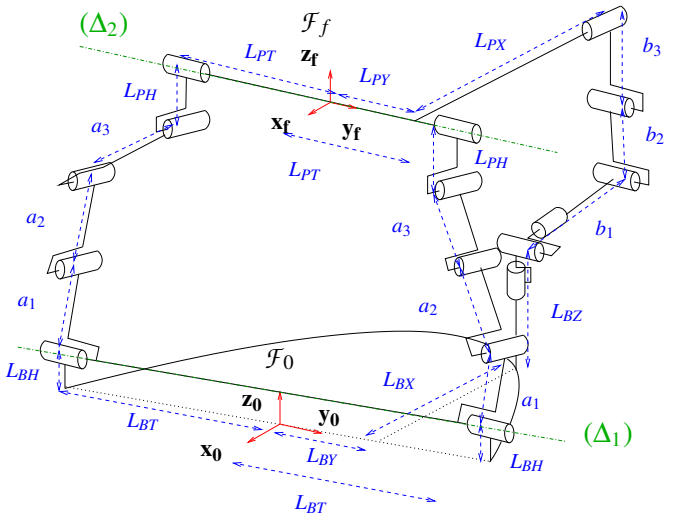

Figure 2. FUNCTIONAL SCHEMATIC OF THE ROBOT

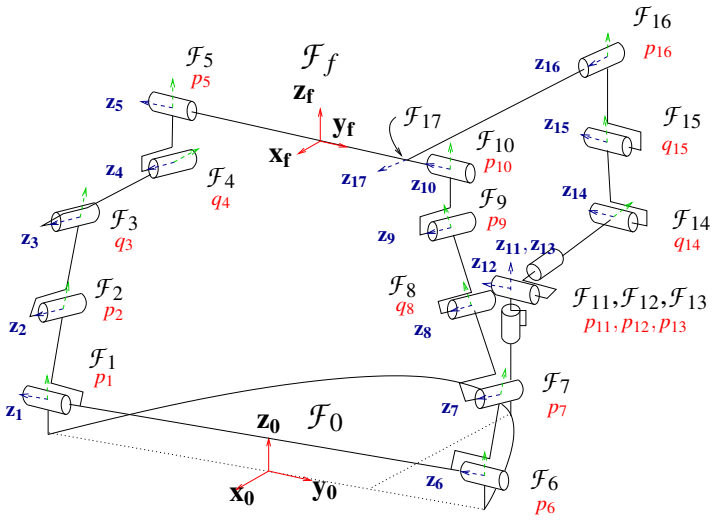

Figure 3. KINEMATIC MODEL OF THE ROBOT

Legs Modeling

Let us first introduce the mathematical notations we use for the modeling.

For any $i, j \in \mathbb{N}$, let C_i be $\cos(\theta_i)$, S_i be $\sin(\theta_i)$, $C_{i,j}$ be $\cos(\theta_i + \theta_j)$, $S_{i,j}$ be $\sin(\theta_i + \theta_j)$, *etc.* Let a rigid frame i be denoted as $\mathcal{F}_i$, and its origin by O_i. Vectors are typed in bold face. The coordinates of a vector $\mathbf{AB}$, expressed in $\mathcal{F}_i$ are denoted as ${}^iAB$. Its components are ${}^iAB_{[x]}$, ${}^iAB_{[y]}$, ${}^iAB_{[z]}$. The associated homogeneous coordinates are ${}^i\underline{AB}$.

Local Product Of Exponentials Formalism. The modified Denavit-Hartenberg (DH) parameterization [11] is undoubtly the most common way to describe serial robots in order to model them. An interesting alternative to the DH description is given by the product of exponential (POE) [12, 13]. This formalism has a comprehensive geometric interpretation and is easy to use both in the case of serial and parallel robots. To model a serial chain of a robot, we use the local product of exponentials (LPOE), as described in [14]. We briefly recall here the principle of this modeling.

We consider a serial mechanism for which the $i-$th joint connects two adjacent links. The frames $\mathcal{F}_{i-1}$ and $\mathcal{F}_i$ are associated to these successive links. The rigid transformation describing the pose of $\mathcal{F}_i$ relative to $\mathcal{F}_{i-1}$ is given by the homogeneous matrix of $SE(3)$:

$$ {}^{i-1}T_i(\theta_i) = \begin{bmatrix} {}^{i-1}R_i & {}^{i-1}O_{i-1}O_i \\ 0 & 1 \end{bmatrix} \qquad (1) $$

where ${}^{i-1}R_i$ and ${}^{i-1}O_{i-1}O_i$ respectively represent the rotation and the translation from $\mathcal{F}_{i-1}$ to $\mathcal{F}_i$. The expression of the transformation using the LPOE is :

$$ {}^{i-1}T_i(\theta_i) = {}^{i-1}T_i(0)\, e^{\widehat{\xi}_i \theta_i} \qquad (2) $$

where ${}^{i-1}T_i(0)$ gives the pose resulting from the fully extended initial configuration of frame $\mathcal{F}_i$ expressed in $\mathcal{F}_{i-1}$ and $\widehat{\xi}_i$ is the matrix associated to a transformation by a twist ξ_i [12, 14]. To simplify the modeling we consider that the initial rotation matrix is identity : ${}^{i-1}R_i = I$. The position θ_i of the $i-th$ joint is denoted as q_i for the actuated joints and as p_i for the passive joints. The $i-th$ joint $\mathbf{z_i}$ axis is oriented as defined on Fig. 3.

As we consider the legs independently, we write their fully extended initial configuration joining frame $\mathcal{F}_0$ to $\mathcal{F}_f$. First, we define the initial configuration of the first leg by Tab. 1. The composition of the elementary transformations gives the forward kinematics of the first chain denoted as gst_1.

Table 1. INITIAL CONFIGURATION OF THE FIRST LEG.

Axis ${}^0z_i$	Joint i center position : ${}^0O_{i-1}O_i$	Joint i position : θ_i
${}^0z_1 = \begin{bmatrix} 0 & -1 & 0 \end{bmatrix}^T$	${}^0O_0O_1 = \begin{bmatrix} 0 & -L_{BT} & L_{BH} \end{bmatrix}^T$	p_1
${}^0z_2 = \begin{bmatrix} 1 & 0 & 0 \end{bmatrix}^T$	${}^0O_1O_2 = \begin{bmatrix} 0 & 0 & a_1 \end{bmatrix}^T$	p_2
${}^0z_3 = \begin{bmatrix} 1 & 0 & 0 \end{bmatrix}^T$	${}^0O_2O_3 = \begin{bmatrix} 0 & 0 & a_2 \end{bmatrix}^T$	q_3
${}^0z_4 = \begin{bmatrix} 1 & 0 & 0 \end{bmatrix}^T$	${}^0O_3O_4 = \begin{bmatrix} 0 & 0 & a_3 \end{bmatrix}^T$	q_4
${}^0z_5 = \begin{bmatrix} 0 & -1 & 0 \end{bmatrix}^T$	${}^0O_4O_5 = \begin{bmatrix} 0 & 0 & L_{PH} \end{bmatrix}^T$	p_5
${}^0z_f = \begin{bmatrix} 0 & 0 & 1 \end{bmatrix}^T$	${}^0O_5O_f = \begin{bmatrix} 0 & L_{PT} & 0 \end{bmatrix}^T$	

Table 2. INITIAL CONFIGURATION OF THE SECOND LEG.

Axis ${}^0z_i$	Joint i center position : ${}^0O_{i-1}O_i$	Joint i position : θ_i
${}^0z_6 = \begin{bmatrix}0 & -1 & 0\end{bmatrix}^T$	${}^0O_0O_6 = \begin{bmatrix}0 & L_{BT} & L_{BH}\end{bmatrix}^T$	p_6
${}^0z_7 = \begin{bmatrix}1 & 0 & 0\end{bmatrix}^T$	${}^0O_6O_7 = \begin{bmatrix}0 & 0 & a_1\end{bmatrix}^T$	p_7
${}^0z_8 = \begin{bmatrix}1 & 0 & 0\end{bmatrix}^T$	${}^0O_7O_8 = \begin{bmatrix}0 & 0 & a_2\end{bmatrix}^T$	q_8
${}^0z_9 = \begin{bmatrix}1 & 0 & 0\end{bmatrix}^T$	${}^0O_8O_9 = \begin{bmatrix}0 & 0 & a_3\end{bmatrix}^T$	p_9
${}^0z_{10} = \begin{bmatrix}0 & -1 & 0\end{bmatrix}^T$	${}^0O_9O_{10} = \begin{bmatrix}0 & 0 & L_{PH}\end{bmatrix}^T$	p_{10}
${}^0z_f = \begin{bmatrix}0 & 0 & 1\end{bmatrix}^T$	${}^0O_{10}O_F = \begin{bmatrix}0 & -L_{PT} & 0\end{bmatrix}^T$	

Table 3. INITIAL CONFIGURATION OF THE THIRD LEG.

Axis ${}^0z_i$	Joint i center position : ${}^0O_{i-1}O_i$	Joint i position : θ_i
${}^0z_{11} = \begin{bmatrix}0 & 0 & 1\end{bmatrix}^T$	${}^0O_0O_{11} = \begin{bmatrix}-L_{BX} & L_{BY} & L_{BZ}\end{bmatrix}^T$	p_{11}
${}^0z_{12} = \begin{bmatrix}0 & -1 & 0\end{bmatrix}^T$	${}^0O_{11}O_{12} = \begin{bmatrix}0 & 0 & 0\end{bmatrix}^T$	p_{12}
${}^0z_{13} = \begin{bmatrix}0 & 0 & 1\end{bmatrix}^T$	${}^0O_{12}O_{13} = \begin{bmatrix}0 & 0 & 0\end{bmatrix}^T$	p_{13}
${}^0z_{14} = \begin{bmatrix}0 & -1 & 0\end{bmatrix}^T$	${}^0O_{13}O_{14} = \begin{bmatrix}0 & 0 & b_1\end{bmatrix}^T$	q_{14}
${}^0z_{15} = \begin{bmatrix}0 & -1 & 0\end{bmatrix}^T$	${}^0O_{14}O_{15} = \begin{bmatrix}0 & 0 & b_2\end{bmatrix}^T$	q_{15}
${}^0z_{16} = \begin{bmatrix}1 & 0 & 0\end{bmatrix}^T$	${}^0O_{15}O_{16} = \begin{bmatrix}0 & 0 & b_3\end{bmatrix}^T$	p_{16}
${}^0z_f = \begin{bmatrix}0 & 0 & 1\end{bmatrix}^T$	${}^0O_{16}O_F = \begin{bmatrix}L_{PX} & -L_{PY} & 0\end{bmatrix}^T$	

The second leg has some parameters linked to the first leg. The forward kinematics of this chain will be gst_2 and its initial configuration is given Tab. 2. The last leg has the its initial configuration given in Tab. 3. Each line of joint parameters gives an homogeneous transform by applying the exponential mapping of twists on $SE(3)$.

KINEMATIC MODELING

The platform configuration should be expressed by five parameters, corresponding to the number of degrees of freedom of the platform. A first solution is to consider : i) the platform origin ${}^0O_f$ with coordinates: $[{}^0O_0O_{f\ [x]}\ {}^0O_0O_{f\ [y]}\ {}^0O_0O_{f\ [z]}]^T$ in $\mathcal{F}_0$; ii) the normal unit vector attached to the platform and pointing upward, with coordinates $[{}^0z_{f\ [x]}\ {}^0z_{f\ [y]}\ {}^0z_{f\ [z]}]^T$ in $\mathcal{F}_0$ (only two degrees of freedom since the norm of the vector is equal to one).

Inverse Kinematics

Angle Between the Base and the First Closed Chain. Let us rewrite the position of point O_f in $\mathcal{F}_1$. We know that the first and second leg lie in the same plane, so that only one angle p_1 can determine ${}^0O_0O_{f\ [x]}$ and ${}^0O_0O_{f\ [z]}$. For a given distance between O_1 and O_f, we have :

$$ {}^0O_1O_{f\ [x]} = -||\mathbf{O_1O_f}||S_1, \tag{3}$$

$$ {}^0O_1O_{f\ [z]} = ||\mathbf{O_1O_f}||C_1. \tag{4}$$

From Fig. 3, we can see that ${}^0O_1O_{f\ [x]} = {}^0O_0O_{f\ [x]}$, and ${}^0O_1O_{f\ [z]} = {}^0O_0O_{f\ [z]} - L_{BH}$. Finally:

$$ p_1 = \arctan2(-{}^0O_0O_{f\ [x]},\ {}^0O_0O_{f\ [z]} - L_{BH}) \tag{5}$$

First Leg. The first leg forward kinematics can be projected in the (O_1, O_6, O_f) plane by premultiplying gst_1 by ${}^1T_0$. Hence the vector $\mathbf{O_5O_f}$ in $\mathcal{F}_1$ should have a null coordinate on ${}^1O_5O_{f\ [x]}$. This will be useful to obtain the angles p_2, q_3 and q_4:

$$ \mathbf{O_5O_f} = \mathbf{O_0O_f} - \mathbf{O_0O_5}, \tag{6}$$

$$ \underline{{}^1O_5O_f} = {}^0T_1 gst_1 \left(I - {}^fT_5\right)[1\ 0\ 0\ 1]^T. \tag{7}$$

As we have the constraint that $\mathbf{z_f}$ is orthogonal to $\mathbf{O_5O_f}$, we obtain:

$$ \left({}^1O_5O_f\right)^T {}^1z_f = L_{PT}\left({}^1z_{f[y]}C_{2,3,4} + ({}^1z_{f[z]}C_1 - {}^1z_{f[x]}S_1)S_{2,3,4}\right) = 0. \tag{8}$$

Then we proceed to the substitution $C_{2,3,4} = \varepsilon\sqrt{1 - {S_{2,3,4}}^2}$ with $\varepsilon \in \{1, -1\}$ in the previous equation. This substitution introduces a new supplementary solution that has mathematically to be considered. Once solved for $S_{2,3,4}$, we have:

$$ S_{2,3,4} = \frac{\varepsilon\, {}^1z_{f[y]}}{\sqrt{{}^1z_{f[y]}^2 + {}^1z_{f[x]}^2 {S_1}^2 - 2\,{}^1z_{f[x]}\,{}^1z_{f[z]}S_1C_1 - {}^1z_{f[z]}^2{S_1}^2 + {}^1z_{f[z]}^2}} \tag{9}$$

A singularity appears when the denominator of $S_{2,3,4}$ is null but this case should not appears since it means that $S_{2,3,4} = 0$ and the platform is perpendicular to the base.

The ε indeterminate represents a symmetric orientation of the platform relative to the base frame along the (O_f,x_0,z_0) plane. Numerically, we find that $\varepsilon = -1$ is for the correct orientation.

Because we only have the sinus of $p_2 + q_3 + q_4 = \Sigma_{2,3,4}$, again two solutions are possible. To solve this, we impose a mechanical constraint: we suppose that the platform vector $\mathbf{z_f}$ makes a maximum angle of $\pm\frac{\pi}{2}$ with the base vector $\mathbf{z_0}$ around the $\mathbf{x_0}$ axis of the base frame. The angle $\arcsin(S_{2,3,4})$ is then entirely defined by its sinus that is in $]-\frac{\pi}{2}, \frac{\pi}{2}[$.

Now we solve for the whole kinematic chain. Let's compute $\mathbf{O_1O_4}$ by two different ways. First by using the leg 1:

$$\begin{aligned} {}^1\underline{O_1O_4}_{|\text{Leg 1}} &= {}^1T_2\,{}^2T_3\,{}^3T_4[1\ 0\ 0\ 1]^T \\ &= \begin{bmatrix} 0 \\ -a_2S_2 - a_3S_{2,3} \\ a_1 + a_2C_2 + a_3C_{2,3,4} \\ 1 \end{bmatrix}. \end{aligned} \tag{10}$$

Then passing by the platform, we have:

$${}^1\underline{O_1O_4}_{|\text{Pl}} = \begin{bmatrix} {}^0O_0O_{f\,[\text{x}]}C_1 + ({}^0O_0O_{f\,[\text{z}]} - L_{BH})S_1 \\ {}^0O_0O_{f\,[\text{y}]} + L_{BT} - L_{PT}C_{2,3,4} + L_{PH}S_{2,3,4} \\ -{}^0O_0O_{f\,[\text{x}]}S_1 + ({}^0O_0O_{f\,[\text{z}]} - L_{BH})C_1 - L_{PT}S_{2,3,4} - L_{PH}C_{2,3,4} \\ 1 \end{bmatrix}. \tag{11}$$

If we sum the square of the Y and Z coordinates in Eqns. (10)-(11), we can obtain:

$$\left({}^1O_1O_{4\,[\text{y}]|\text{Pl}}\right)^2 + \left({}^1O_1O_{4\,[\text{z}]|\text{Pl}}\right)^2 = {a_2}^2 + 2a_2a_3C_3 + a_3^2, \tag{12}$$

that allows to compute:

$$q_3 = \arccos\left(\frac{-\left({}^1O_1O_{4\,[\text{y}]|\text{Pl}}\right)^2 - \left({}^1O_1O_{4\,[\text{z}]|\text{Pl}}\right)^2 + a_2^2 + a_3^2}{2a_2a_3}\right). \tag{13}$$

Then we obtain p_2 by the substitution: $S_2 = \frac{2t_2}{1+t_2^2}$ and $C_2 = \frac{1-{t_2}^2}{1+{t_2}^2}$ in Eqn. (10). After this substitution, we solve for t_2 and have:

$$t_2 = \frac{a_2 + a_3C_3 \pm \sqrt{a_2^2 + 2a_2a_3C_3 + a_3^2 - \left({}^1O_1O_{4\,[\text{y}]|\text{Pl}}\right)^2}}{a_3S_3 - {}^1O_1O_{4\,[\text{y}]|\text{Pl}}}. \tag{14}$$

A singularity is shown when $a_3S_3 = {}^1O_1O_{4\,[\text{y}]|\text{Pl}}$. This means that O_1 and O_4 are coincident, which should not happen in reality. A final step gives:

$$p_2 = 2\arctan(t_2), \tag{15}$$

and finally:

$$q_4 = \Sigma_{234} - p_2 - q_3. \tag{16}$$

Second Leg. We use the same type of resolution for the second leg. We now work on vector $\mathbf{O_{10}O_f}$ in frame $\mathcal{F}_6$. The orthogonal constraint gives the following equation:

$$\left({}^6O_{10}O_f\right)^T {}^6z_f = L_{PT}\,{}^6z_{\text{y}}C_{7,8,9} + L_{PT}(-{}^6z_{\text{x}}.S_1 + {}^6z_{\text{z}}C_1)S_{7,8,9} = 0. \tag{17}$$

Then we solve for $S_{7,8,9}$:

$$S_{7,8,9} = \frac{\varepsilon\,{}^6z_{f\,[\text{y}]}}{\sqrt{{}^6z_{f\,[\text{y}]}^2 + {}^6z_{f\,[\text{x}]}^2S_6^2 - 2S_6C_6\,{}^6z_{f\,[\text{x}]}^2\,{}^6z_{f\,[\text{z}]}^2 - {}^6z_{f\,[\text{z}]}^2S_6^2 + {}^6z_{f\,[\text{z}]}^2}}. \tag{18}$$

This gives another supplementary singularity and two solutions for $S_{7,8,9}$. As before, $\varepsilon = -1$ and again two solutions exists for $\Sigma_{7,8,9} = p_7 + q_8 + p_9$. This is solved because of mechanical constraints: $S_{7,8,9} \in]-\frac{\pi}{2}, \frac{\pi}{2}[$ and $\Sigma_{7,8,9} = \arcsin(S_{7,8,9})$.

The kinematic chain is solved again by computing ${}^6\underline{O_6O_9}_{|\text{Pl}}$ and ${}^6\underline{O_6O_9}_{|\text{Leg 2}}$ as done before. This gives an equation after equaling the squared sum of Y and Z coordinates :

$$\left({}^6O_6O_{9\,[\text{y}]|\text{Pl}}\right)^2 + \left({}^6O_6O_{9\,[\text{z}]|\text{Pl}}\right)^2 = {a_2}^2 + 2a_2a_3C_8 + {a_3}^2, \tag{19}$$

from which we have:

$$q_8 = \pi - \arccos\left(\frac{-\left({}^6O_6O_{9\,[\text{y}]|\text{Pl}}\right)^2 - \left({}^6O_6O_{9\,[\text{z}]|\text{Pl}}\right)^2 + {a_2}^2 + {a_3}^2}{2a_2a_3}\right). \tag{20}$$

As before, p_7 is obtained by the substitution $S_7 = \frac{2t_7}{1+t_7^2}$:

$$t_7 = \frac{-a_2 - a_3C_8 \pm \sqrt{{a_2}^2 + 2a_2a_3C_8 + {a_3}^2 - \left({}^6O_6O_{9\,[\text{y}]|\text{Pl}}\right)^2}}{a_3S_6 - {}^6O_6O_{9\,[\text{y}]|\text{Pl}}}. \tag{21}$$

We find a singularity in t_7 with the same meaning as for leg one. Then :

$$p_7 = 2\arctan(t_7), \tag{22}$$

and finally:

$$p_9 = \Sigma_{7,8,9} - p_7 - q_8. \tag{23}$$

Platform Angle. For p_5 (or p_{10}), which is the last angle that has to be found, we compute ${}^0z_f$ by using the first leg forward kinematics. This gives:

$${}^0z_f = \begin{bmatrix} -C_1S_5 - S_1C_5 \\ -C_5S_{2,3,4} \\ -S_1S_5 + C_1C_5C_{2,3,4} \end{bmatrix}. \tag{24}$$

As this vector is known, we compute C_5 and S_5 that define completely the angle:

$$p_5 = \arctan 2\left(-C_1\,{}^0z_{[\text{x}]} - S_1\,{}^0z_{[\text{z}]}, \frac{-S_1\,{}^0z_{[\text{x}]} + C_1\,{}^0z_{[\text{z}]}}{C_{2,3,4}}\right). \tag{25}$$

A singularity is possible if $C_{2,3,4} = 0$. This is the case when $\mathbf{z_f}$ is collinear with $\mathbf{y_0}$.

Third Leg. Once we have solved the first 6-bar linkage, we can define the platform orientation thanks to $\mathbf{x_f}$, $\mathbf{y_f}$ and $\mathbf{z_f}$. The last leg has six degrees of freedom and can be solved by position/orientation considerations.

The first passive parameter to be found is p_{16}. It is the angle between the plane $(O_f, \mathbf{x_f}, \mathbf{z_f})$ and the plane $(O_{16}, \mathbf{z_{16}}, \mathbf{y_{16}})$. This angle is also the angle between the Y component and Z component of ${}^fO_{13}O_{16}$. As :

$${}^fO_{13}O_{16} = {}^fR_0\,{}^0O_{13}O_f + {}^fO_fO_{16}, \tag{26}$$

we get:

$$\begin{aligned} p_{16} = \arctan 2\big(((L_{BX} + {}^0O_0O_{f_{[x]}})S_1 - C_1)S_{2,3,4} + \\ (L_{BY} - {}^0O_0O_{f_{[y]}})C_{2,3,4} - L_{PY}, \\ {}^0z_{[x]}({}^0O_0O_{f_{[x]}} + L_{BX}) + {}^0z_{[y]}({}^0O_0O_{f_{[y]}} - L_{BY}) + \\ {}^0z_{[z]}({}^0O_0O_{f_{[z]}} - L_{BZ})\big). \end{aligned} \tag{27}$$

The last two parameters are q_{14} and q_{15}. They are obtained by first computing the vector $\mathbf{O_{13}O_{16}}$ using the forward kinematics of the leg and then by computing it using frames $\mathcal{F}_0$, $\mathcal{F}_f$, and $\mathcal{F}_{16}$. This is similar to the previous calculus for legs one and two:

$${}^{16}O_{13}O_{16[x]} = -b_1S_{14,15} + b_2S_{15}, \tag{28}$$

$${}^{16}O_{13}O_{16[z]} = -b_1C_{14,15} - b_2C_{15}, \tag{29}$$

$$\left({}^{16}O_{13}O_{16[x]}\right)^2 + \left({}^{16}O_{13}O_{16[z]}\right)^2 = {b_2}^2 + 2b_1b_2C_{14} + {b_1}^2. \tag{30}$$

Hence we have two solutions for q_{14}. But, because of mechanical design, q_{14} is always in $\in [0,\pi]$ and so:

$$q_{14} = \arccos\left(\frac{\left({}^{16}O_{13}O_{16[x]}\right)^2 + \left({}^{16}O_{13}O_{16[z]}\right)^2 - {b_2}^2 - {b_1}^2}{2b_1b_2}\right). \tag{31}$$

Finally, we substitute $t_{15} = \tan\frac{q_{15}}{2}$ in Eqn. (28) and Eqn. (29). After computations and solving for t_{15}, we obtain:

$$q_{15} = -2\arctan\left(\frac{b_1C_{14} + b_2 \pm \sqrt{b_1^2 + b_2^2 + 2b_1b_2C_{14} - \left({}^{16}O_{13}O_{16[x]}\right)^2}}{-b_1S_{14} + {}^{16}O_{13}O_{16[x]}}\right), \tag{32}$$

which gives another singularity when $b_1S_{14} = {}^{16}O_{13}O_{16[x]}$.

Forward Kinematics

First 6-bar Linkage. We study the first 6-bar linkage in $\mathcal{F}_1$. This linkage has three degrees of freedom in the plane (O_1,$\mathbf{z_1}$,$\mathbf{y_1}$): rotation and position. In this linkage we have three actuated degrees of freedom q_3, q_4 and q_8. Hence we should be able to completely define its configuration.

When only p_2, q_3 and q_4 are given, a point on the first leg draws a circle about the line (Δ_1) due to the angle p_1. The point O_2 also draws a circle when p_1 changes, but if we place our referential in $\mathcal{F}_1$, this point is static. Since O_9 lies in the same plane and p_3 does not change their positions, we can consider that only p_2 determines the position of O_9 in $\mathcal{F}_1$, and O_9 describes a circle centered on O_2.

We consider the radius of this circle to be a constant distance : $||\mathbf{O_2O_9}||$ which can be written thanks to the projection of $\mathbf{O_2O_9}$ in $\mathcal{F}_1$:

$${}^1O_2O_9 = \begin{bmatrix} 0 \\ 2L_{PT}C_{2,3,4} - a_2S_2 - a_3S_{2,3} \\ 2L_{PT}S_{2,3,4} + a_2C_2 + a_3C_{2,3} \end{bmatrix}. \tag{33}$$

Then:

$$||\mathbf{O_2O_9}||^2 = 4L_{PT}\left(L_{PT} + a_2S_{3,4} + a_3S_4\right) + a_2^2 + a_3^2 + 2a_2a_3C_3\,. \tag{34}$$

The second leg has the same property, *i.e.* each point generates a circle about (Δ_1). If we suppose that q_8 is a constant, the movement of O_9 in $\mathcal{F}_6$ is a circle centered on O_7 with a radius of $||\mathbf{O_7O_9}||$. As before:

$$||\mathbf{O_7O_9}||^2 = a_2^2 + a_3^2 + 2a_2a_3C_8. \tag{35}$$

Then we can have the intersection between these two circles. Geometrically, this intersection is O_9 and its position is expressed in $\mathcal{F}_1$ by:

$$({}^1O_1O_{9[y]})^2 + ({}^1O_1O_{9[z]})^2 = ||\mathbf{O_2O_9}||^2, \tag{36}$$

$$\left({}^1O_1O_{9[y]} - 2L_{BT}\right)^2 + ({}^1O_1O_{9[z]})^2 = ||\mathbf{O_7O_9}||^2. \tag{37}$$

We subtract Eqn. (37) from Eqn. (36) and solve for ${}^1O_1O_{9[y]}$ and ${}^1O_1O_{9[z]}$:

$${}^1O_1O_{9[y]} = \frac{L_{BT}^2 + ||\mathbf{O_2O_9}||^2 - ||\mathbf{O_7O_9}||^2}{4L_{BT}}, \tag{38}$$

$${}^1O_1O_{9[z]} = \pm\sqrt{||\mathbf{O_2O_9}||^2 - ({}^1O_1O_{9[y]})^2}. \tag{39}$$

Here two symmetrical solutions are possible, but in reality, only ${}^1O_1O_{9[z]} > 0$ will be kept. As we know the position of O_9, we deduce the angle p_2 of the first leg from Eqn. (33) :

$$\begin{aligned} {}^1O_1O_{9[y]} &= \underbrace{(-a_3S_3 + 2L_{PT}C_{3,4})}_{t_1}C_2 + \underbrace{(-a_2 - a_3C_3 - 2L_{PT}S_{3,4})}_{t_2}S_2, \\ {}^1O_1O_{9[z]} &= -t_2C_2 + t_1S_2. \end{aligned} \tag{40}$$

We can finally deduce C_2 and S_2, which gives p_2:

$$p_2 = \arctan 2\left(\frac{t_1\,{}^1O_1O_{9[z]} + t_2\,{}^1O_1O_{9[y]}}{t_1^2 + t_2^2}, \frac{-t_2\,{}^1O_1O_{9[z]} + t_1\,{}^1O_1O_{9[z]}}{t_1^2 + t_2^2}\right). \tag{41}$$

With the same method, we get for p_9:

$$\begin{aligned} {}^1O_1O_{9[y]} &= \underbrace{-a_3S_3}_{t_3}C_9 + \underbrace{(-a_2 - a_3C_3)}_{t_4}S_9 + 2L_{BT}, \\ {}^1O_1O_{9[z]} &= -t_4C_9 + t_3S_9 + 2L_{BT}. \end{aligned} \tag{42}$$

Once solved :

$$p_9 = \arctan 2\left(\frac{t_3\,{}^1O_1O_{9[z]} + t_4\,{}^1O_1O_{9[y]} - 2t_4L_{BT}}{t_3^2 + t_4^2}, \frac{-t_4\,{}^1O_1O_{9[z]} + t_3\,{}^1O_1O_{9[y]} - 2t_3L_{BT}}{t_3^2 + t_4^2}\right). \tag{43}$$

The last parameter to be found is p_4. As the linkage is a loop, we have:

$$p_7 = p_2 + q_3 + q_4 - p_9 - q_8. \tag{44}$$

Second 4-bar linkage. When q_{14} and q_{15} are fixed, the vector $\mathbf{O_{13}O_{17}}$ becomes a constant length that can be identified as the entire third leg (see Fig. 3). Hence O_{17} is positioned on a sphere centered on O_{13} with a radius $||\mathbf{O_{13}O_{17}}||$. This length is obtained and computed thanks to the forward kinematics of the third leg by :

$$^{13}\underline{O_{13}O_{17}} = {}^{13}T_{14}\,{}^{14}T_{15}\,{}^{15}T_{16}\,{}^{16}T_{17}\,[1\ 0\ 0\ 1]^T, \tag{45}$$

$$= \begin{bmatrix} L_{PX}C_{14,15} - b_3S_{14,15} - b_2S_{14} \\ 0 \\ L_{PX}S_{14,15} + b_3C_{14,15} + b_2S_{14} + b_1 \\ 1 \end{bmatrix}. \tag{46}$$

On the other hand, the first 6-bar linkage is already fully defined, and we obtain the position of point O_{17} by computing the forward kinematics of the first leg and by an appropriate proportional adjustment:

$$\mathbf{O_1O_{17}} = \frac{L_{BT}+L_{PY}}{L_{PT}}(\mathbf{O_1O_f} - \mathbf{O_1O_5}). \tag{47}$$

In $\mathcal{F}_1$:

$$^1O_1O_{17} = \begin{bmatrix} 0 \\ -a_2S_2 - a_3S_{2,3} - L_{PH}S_{2,3,4} + (L_{PT}+L_{PY})C_{2,3,4} \\ a_1 + a_2C_2 + a_3C_{2,3} + L_{PH}C_{2,3,4} + (L_{PT}+L_{PY})S_{2,3,4} \end{bmatrix}. \tag{48}$$

Because of the free joint p_1, O_{17} draws a circle about (Δ_1). If we write $\mathcal{P}(O_{17})$ the orthogonal projection of O_{17} on (Δ_1), then O_{17} lies on the circle centered on $\mathcal{P}(O_{17})$ with radius $||\mathcal{P}(\mathbf{O_{17}})\mathbf{O_{17}}||$. The first problem is to find the position of $\mathcal{P}(O_{17})$ in $\mathcal{F}_O$. We know that $\mathcal{P}(O_{17})$ has the same Y coordinate as $^0O_{17}$ but its X and Z coordinates are those of O_1 in $\mathcal{F}_0$, so:

$$^0\mathcal{P}(O_{17}) = \begin{bmatrix} 0 \\ -a_3S_{2,3} - L_{PH}S_{2,3,4} + (L_{PT}+L_{PY})C_{2,3,4} - L_{BT} \\ L_{BH} \end{bmatrix}. \tag{49}$$

If we define a new coordinate frame $\mathcal{F}_{\mathcal{P}(O_{17})} = (O\mathcal{P}(O_{17}), \mathbf{x_0}, \mathbf{y_0}, \mathbf{z_0})$, we can rewrite all the unknown terms in this frame coordinate attached to $\mathcal{P}(O_{17})$ with the same orientation as $\mathcal{F}_0$. The equation of the circle becomes:

$$||\mathcal{P}(\mathbf{O_{17}})\mathbf{O_{17}}||^2 = (^0O_0O_{17[\mathrm{x}]})^2 + (^0O_0O_{17[\mathrm{z}]})^2 \tag{50}$$

and the sphere of the third leg becomes:

$$||\mathbf{O_{13}O_{17}}||^2 = (^0O_0O_{17[\mathrm{x}]} + L_{BX})^2 + (^0O_0O_{17[\mathrm{z}]} - L_{BZ} + L_{BH})^2 + (L_{BY} - {}^0O_0O_{17[\mathrm{y}]})^2. \tag{51}$$

Then of Eqns.(50) and (51) lead to an equation of the form: $a(^0O_0O_{17[\mathrm{z}]})^2 + b(^0O_0O_{17[\mathrm{z}]}) + c = 0$, with $a,\ b,\ c \in \mathbb{R}$. Thus we have 2 solutions for $^0O_0O_{17[\mathrm{z}]}$ and therefore 2 solutions for $^0O_0O_{17[\mathrm{x}]}$. Once solved, we get the position of O_{17} in $\mathcal{F}_0$. Finally :

$$p_1 = \arctan 2(^0O_0O_{17[\mathrm{x}]}, {}^0O_0O_{17[\mathrm{z}]} - L_{BH}). \tag{52}$$

Hence the position of O_f is determined in $\mathcal{F}_O$.

The Platform Vector $\mathbf{z_f}$. To obtain the full attitude of the platform, we do need to find the $\mathbf{z_f}$ vector. This is equivalent to find the position of point O_{16} in $\mathcal{F}_O$ if we remember that :

$$\mathbf{z_f} = \frac{\mathbf{O_fO_{17}} \times \mathbf{O_{17}O_{16}}}{||\mathbf{O_fO_{17}} \times \mathbf{O_{17}O_{16}}||}. \tag{53}$$

This problem is similar to the previous one and the way to solve it is almost the same: we search for the intersection between a circle generated by O_{16} about the axis $\mathbf{O_5O_{17}}$ with a radius of $||\mathbf{O_{17}O_{16}}||$ and a sphere generated by O_{16} centered on O_{13} with a radius of $||\mathbf{O_{13}O_{16}}||$.

The solution of this problem is not described because of lack of space, but it leads to at least two results that are mechanically possible. This is a common problem in forward kinematics of parallel structures, and we cannot *a priori* solve the issue by verifying each choice and comparing the pose. However, the two solutions are easily separatable as one gives a solution where the third leg lies inside the operating-space and the other solution, symmetrically, gives a solution outside the operating-space.

Approximated Jacobian

The computation of the Jacobian matrix of the system if of great importance both for conception and control. Indeed, for given operational force, the torque on each actuated joint can be computed using the classical equation:

$$\tau = J^T F. \tag{54}$$

This is very useful for e.g. optimization of the length parameters against the rigidity. The well known singularity condition has also a great importance since the condition number (smallest singular value of J divided by largest one) can give a good measure of the manipulability of the robot at an operating point. In our particular case, we cannot easily derive the equation of neither the inverse nor the forward kinematics solution. Too many dependencies are made on the many passive joints parameters. We thus had to compute the approximation of the Jacobian matrix, based on the numerical derivative of the forward kinematics solution.

RESULTS

The inverse kinematic inputs $^0O_00_f$ and ^0z_f can be transformed to special spherical-like coordinates, very comfortable for representing the configuration of the platform :

the entry point: $^0O_0E = [E_{\mathrm{x}}\ E_{\mathrm{y}}\ E_{\mathrm{z}}]^T$;
two rotation angles around this entry point: (ϕ, θ);
a constant platform altitude:(ρ).

One rotation is made about the $\mathbf{x_0}$ axis (ϕ), and about the $\mathbf{y_0}$ axis θ.

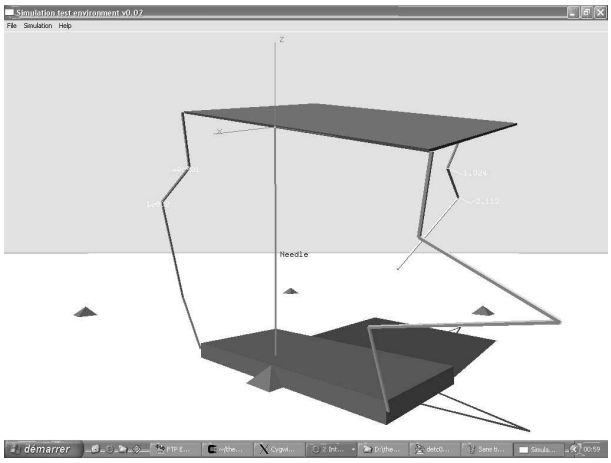

Figure 4. NUMERICAL SIMULATION USING A DYNAMIC ENGINE

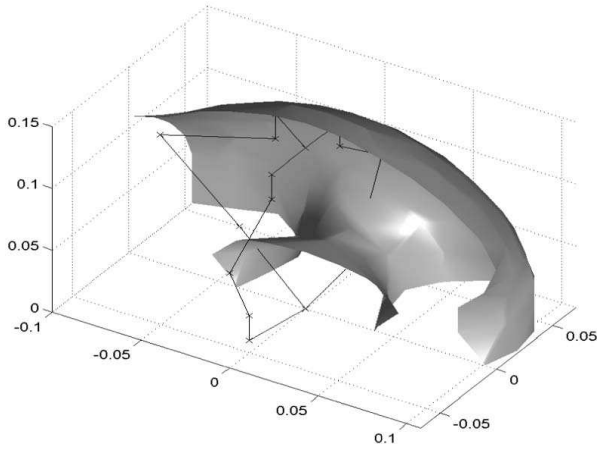

Figure 5. SIMPLIFIED WORKSPACE OF THE ROBOT

The position of the entry point and ρ are redundant information. So we consider ρ to be a constant that should not change over time (it is the altitude relative to the entry point). Once given this additional constraint, we can easily transform one configuration to another by the reversible transformation:

$$ {}^0z_f = \begin{bmatrix} \cos(\theta)\sin(\phi) \\ -\sin(\theta) \\ \cos(\theta)\cos(\phi) \end{bmatrix}, \quad {}^0O_0O_f = {}^0O_0E + \rho \times {}^0z_f. \qquad (55) $$

Numerical Simulation Using a Dynamic Engine

In order to verify the possible motions of the mechanism, we used a numerical dynamic engine in C++ (Open Dynamic Engine) to build a virtual mechanism that contains the same configuration of the joints as our robot has (Fig. 4).

We implemented the inverse and forward kinematics to verify the positioning (${}^0O_0E = [E_x\ E_y\ E_z]^T$) and orientation (ϕ,θ,(ρ)) part of our model and we tested it by applying gravity force to see how the mechanism reacts. The simulations confirm that the kinematics models are well solved. The structure stays rigid even when force is applied on the platform. The lacks of this simulation are that no collisions are checked when the platform moves and no planning has been made for trajectories. This is an issue to be solved.

Reachable Workspace

The workspace is defined as the reachable 3D space of the platform origin O_f for a given configuration of ${}^0z_f$. This robot has five degrees of freedom, and therefore its reachable workspace is difficult to draw . We present here only a particular configuration for ${}^0z_f$: $\theta = 0$, $\phi = 0$. A Matlab plot of the half envelope of the workspace is given on Fig. 5. As we can see, the workspace is almost spherical.

Figure 6. GENERAL LAYOUT

Real Prototype.

CT-Bot is the name given to the physical prototype of which building is under way. In this section we survey the main steps of the prototype design with some details concerning the mechanical structure and the drive system. Figure 6 depicts the general layout of the patient and the robotic device before he enters the CT-scan ring.

The design process has been conducted with an extensive usage of CAD system. Starting from the structural description of the robot (mechanism topology, number of bodies, type of joints) we modeled the robot to define its kinematics. At this stage, the parts' geometry is just a set of lines and points that represents the robot skeleton.

Then the different components were designed with a direct

Figure 7. CT-BOT IN THE CT-SCAN

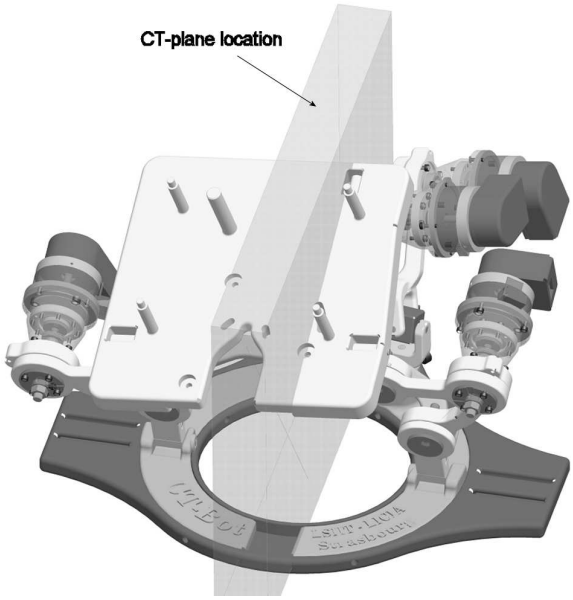

Figure 8. CT-BOT CAD-MODEL

relationship with the robot skeleton. This top-down design approach takes advantage of the initial parameterization and enables to change characteristic dimensions on the structure without re-designing the parts.

Mechanical Structure of the CT-Bot Prototype. A robot base support is attached with straps on the patient body. The robot itself is then oriented and fixed on the base support. This feature allows to choose the best initial configuration according to the intervention objective.

In the mechanical design of the links we used bearings to limit friction and backlash. A special care was taken to increase structural stiffness of the system.

Figures 7 and 8, with the robot CAD model environment and in the physical prototype, illustrate how we placed the third leg of the robot at a certain distance away from the $(O_0, \mathbf{x_0}, \mathbf{y_0})$ plane to limit the number of non-plastic parts in the CT-plane. Similarly we oriented actuation units of the third leg.

Drive System. Each actuation unit comprises a gear housing specifically designed for this application, an Harmonic Drive reduction gearing, an ultrasonic motor and an incremental encoder. Ultrasonic motors have several advantages over other type of actuators including :

a good torque to weight ratio ;
a low rotational speed ;
a high holding torque when not powered.

These features are important for our application from the point of view of the effort to be exerted by the robot and the required safety for this medical device. In case of control failure, the robot holding the needle will remain motionless.

The resulting actuation unit has an outer size included in a cylinder of 75 mm in length and 50 mm in diameter.

Manufacturing. Most of the parts composing the robot have been obtained through rapid prototyping with a laser sintering system. This enables to move directly from CAD files to functional plastic parts in a fraction of the time required for traditional machining and tooling processes. The material employed is glass-filled polyamide powder to comply with the CT-Scan imaging requirements.

So far, the following elements have been achieved on the prototype :

construction of the different robot components ;
mechanical assembly of the robot.

The forthcoming stages concerning the physical prototype include the resolution of sterilization-related issues. These constraints were present from the beginning in the design process and practical solutions are to be implemented to pass medical approval. Some preliminary orientations have already been chosen.

Another important subject is the needle insertion tool to be mounted as end-effector on the platform. This system comprises force sensor and will be crucial for task execution.

CONCLUSION

We have presented a new five-degree-of-freedom parallel manipulator intended to help practitioners in percutaneous interventions realized under X-rays imaging devices. These medical

procedures imply many strong constraints on the robotic assistant such as transparency to X-rays, compactness, stiffness and safety.

The modeling of the mechanism has been conducted using the local product of exponentials formalism. Numerical simulations on a wire-frame system enabled to check the main limits of the operational workspace. The results obtained from inverse kinematic analysis were input data to the design process. Starting from topological and dimensional description of the structure, a fully parametric CAD model of the robot has been constructed. This model helped to iteratively improve the design and take into account the technical limitations (actual part geometry, mechanical stops).

As a current result, a physical prototype has been built. Remaining tasks include cabling, electrical connection and construction of the insertion tool to be mounted as end-effector on the platform.

ACKNOWLEDGMENT The authors wish to thank the Alsace Region for the financial support of this research work.

REFERENCES

[1] Gangi, A., and Dietemann, J.-L., 1994. *Tomodensimétrie Interventionnelle*. Editions Vigot, PARIS.

[2] Stoianovici, D., Cadeddu, J. A., R. D. Demaree, H. A. B., Taylor, R. H., Whitcomb, L. L., and Kavoussi, L. R., 1997. "A novel mechanical transmission applied to percutaneous renal access". *Proceedings of the ASME Dynamic Systems and Control Division,* **DSC-Vol. 61** , pp. 401–406.

[3] Yanof, J., Haaga, J., et al., 2001. "CT-integrated robot for interventional procedures: Preliminary experiment and computer-human interfaces". Computer Aided Surgery (6) , pp. 352–359.

[4] Fichtinger, G., DeWeese, T. L., Patriciu, A., Tanacs, A., Mazilu, D., Anderson, J. H., Masamume, K., Taylor, R. H., and Stoianovici, D., 2002. "Robotically assisted prostate biopsy and therapy with intra-operative CT guidance". *Journal of Academic Radiology,* **9** , pp. 60–74.

[5] Shi, M., Liu, H., and Tao, G., 2002. "A stereo-fluoroscopic image-guided robotic biopsy scheme". IEEE Transactions on Control Systems Technology, **10** (3) May , pp. 309–317.

[6] Maurin, B., Piccin, O., Bayle, B., Gangloff, J., de Mathelin, M., Zanne, P., Doignon, C., Gangi, A., and Soler, L., 2004. "A new robotic system for CT-guided percutaneous procedures with haptic feedback". In Proceedings of the 2004 Computer Assisted Radiology and Surgery Congress (To appear), CARS'04.

[7] Simone, C., and Okamura, A. M., 2002. "Modeling of needle insertion forces for robot-assisted percutaneous therapy". In Proceedings of the 2002 IEEE International Conference on Robotics and Automation, ICRA'02, pp. 2085–2091.

[8] Maurin, B., Barbe, L., Bayle, B., Zanne, P., Gangloff, J., de Mathelin, M., Gangi, A., and Forgionne, A., 2004. "In vivo study of forces during needle insertions". In Proceedings of the 2004 Medical Robotics, Navigation and Visualisation Scientific Workshop (To appear), MRNV'04.

[9] Hunt, K., 1978. *Kinematic Geometry of Mechanisms*. Oxford Engineering Series, Clarendon Press.

[10] Tsai, L. W., 2001. *Mechanism Design : enumeration of kinematic structures according to function*. Mechanical Engineering series. CRC Press.

[11] Khalil, W., and Kleinfinger, J., 1986. "A new geometric notation for open and closed loop robots". In Proceedings of the 1986 IEEE International Conference on Robotics and Automation, pp. 75–79.

[12] Murray, R. M., Li, Z., and Sastry, S. S., 1994. *A Mathematical Introduction to Robotic Manipulation*. CRC Press.

[13] Park, F. C., 1994. "Computational aspects of the product-of-exponentials formula for robot kinematics". IEEE Transactions on Automatic Control, **39** (3) March , pp. 643–467.

[14] Yang, G., Chen, I. M., Lim, W. K., and Yeo, S. H., 1999. "Design and kinematic analysis of modular reconfigurable parallel robots". In Proceedings of the 1999 IEEE International Conference on Robotics and Automation, pp. 2501–2506.